metals

MDPI

Article

Tribological Behavior of AA1050H24-Graphene Nanocomposite Obtained by Friction Stir Processing

Julio Blanco Fernandez [1,*], Emilio Jimenez Macias [2], Juan Carlos Saenz-Diez Muro [2], Lorenzo S. Caputi [3], Domenico Miriello [4], Raffaella De Luca [4], Angel Sanchez Roca [5] and Hipólito Domingo Carvajal Fals [5]

1 Mechanical Engineering Department, La Rioja University, C/San José de Calasanz 31, 26004 Logrono, Spain
2 Electrical Engineering Department, La Rioja University, C/San José de Calasanz 31, 26004 Logrono, Spain; emilio.jimenez@unirioja.es (E.J.M.); juan-carlos.saenz-diez@unirioja.es (J.C.S.-D.M.)
3 Surface Nanoscience Group, Department of Physics, University of Calabria, Via P. Bucci, 87036 Rende, Italy; lorenzo.caputi@fis.unical.it
4 Department of Biology, Ecology and Earth Sciences, University of Calabria, Via P. Bucci, 87036 Rende, Italy; miriello@unical.it (D.M.); raffaella.deluca@unical.it (R.D.L.)
5 Materials and Manufacturing Department, Faculty of Mechanical Engineering, Universidad de Oriente, Santiago de Cuba 90400, Cuba; asroca@yahoo.com (A.S.R.); hcf151@yahoo.es (H.D.C.F.)
* Correspondence: julio.blanco@unirioja.es; Tel.: +34-941-299478

Received: 29 December 2017; Accepted: 2 February 2018; Published: 6 February 2018

Abstract: The tribological behavior of a new composite material containing graphene nanosheets (GNS) is presented. The composite material was obtained by Friction Stir Processing, using as metallic matrix the AA1050-H24 alloy. Different tool rotation and advancing speeds were tested in friction stir processing (FSP). The worn surfaces of obtained materials were analyzed by Scanning Electron Microscopy (SEM). Raman spectroscopy demonstrated that graphene reinforcements are successfully mixed into the aluminum matrix. The results proved the feasibility of using GNSs to obtain nanocomposites by FSP. The coefficient of friction of the aluminum alloy was 0.57, decreasing to 0.38 for the nanocomposite GNSs/AA1050. These values decrease for samples obtained at lower tool rotation speeds. The weight losses of the composites are less than that of unreinforced AA1050-H24 alloy for conditions with lower advancing speeds (40 and 60 mm/min) and 1120 rpm.

Keywords: graphene; friction stir; wear; nanocomposites

1. Introduction

Graphene, the perfect two-dimensional lattice of carbon atoms, has been the focus of attention in recent years, mainly due to its excellent mechanical and physical properties, such as high Young's modulus (1 TPa), high fracture strength (125 GPa), and extreme electrical and thermal conductivity [1–5]. Graphene has also excellent friction and wear resistance, which has turned it into a very attractive material for several applications in nanotechnology [6–10]. Specifically, Lee et al. [10] studied the tendency towards friction decrease with the increase in the number of layers of multilayer graphene. Graphene nanosheets (GNSs), which are composed of a small number of graphene layers, have properties similar to those of single-layer graphene, but are much easier to produce. GNSs have high potential in the nanocomposites area: the high fracture strength of graphene makes it an ideal reinforcement for composite materials [2,6]. Wang et al. [3] fabricated, for the first time, aluminum matrix composites strengthened with GNSs by means of a viable methodology based on flake powder metallurgy. A tensile strength of 249 MPa was achieved in the composite reinforced with only 0.3 wt % GNSs, which was enhanced by 62% with respect to the unreinforced Al matrix. Furthermore, composites of graphene platelets and powdered Al were made using ball milling, hot isostatic

pressing, and extrusion [11]. This research showed that graphene is prone to form aluminum carbide (Al_4C_3) during the processing, which lowers the hardness and tensile strength of aluminum. Close attention should be paid to the processing temperatures, in order to avoid the formation of aluminum carbide [11,12].

Friction-stir processing (FSP) is a solid-state processing technique used to obtain a fine-grained and recrystallized microstructure [13]. Although FSP has mainly been used as a grain refinement technique, it is also a very attractive process for creating composites. SiC/Al surface composites were fabricated by FSP, obtaining a homogeneous distribution of the SiC particles in the Al matrix [13]. Some innovative research projects have used FSP to produce composites based on carbon nanotubes (CNTs). In those works, several holes were drilled into a metallic plate and then filled with CNTs and treated by FSP [14]. Alternatively, CNTs powder was introduced into a long groove on the metal surface before to FSP treatment [14,15]. Morisada et al. [16] found that the dispersion of multi-walled CNTs is related to the travel speed of the rotating tool in FSP; a good dispersion was obtained at 1500 rpm. Lim et al. [9] confirmed that increasing the tool rotation speed from 1500 to 2500 rpm and increasing the tool shoulder penetration depth improved the homogeneity of the nanotubes' distribution in the Al-alloy matrix. Izadi et al. [15] proved, by transmission electron microscopy (TEM), that the reinforced phase was uniformly distributed after three FSP passes, but the thermo-mechanical cycles destroyed the tubular structure of the CNTs, with the formation of polyaromatic and turbostratic carbon structures along with Al_4C_3.

The study of the tribological behavior of the graphene nanocomposites is innovative and important due to the high demand in nanotechnology applications [7]. Li et al. [17] proved that the adherence to the substrate has a substantial effect in the friction behavior of graphene, being the interface between graphene and the surface a crucial factor. When the force is increased during friction, the links of the carbon atoms in the sub-layers of graphene can be broken, resulting in bi- or multi-wear layers of graphene. The shear of the interfaces of graphene layers occurs due to the rupture of the surface adhesion forces, such as Van der Waals type, capillary, electrostatic, and chemical bonding [7]. Deng et al. [18] demonstrated that increasing the number of layers decreases the friction coefficient of graphene, when it is adhered to the substrate.

Few studies have been published on nanocomposites containing graphene obtained by FSP. Jeon et al. [19] fabricated graphene-aluminum metal matrix composites (MMCs) by FSP, applying graphene reinforcement in the form of graphene oxide (GO)/water colloid. Based on Raman measurements, the authors demonstrated that graphene was successfully mixed into the aluminum matrix by the intense stirring during FSP. The experimental results showed that the thermal conductivity of the graphene/Al MMC was increased more than 15% in comparison to the aluminum matrix.

The research and development of GNS-based nanocomposites is an important factor in the practical application of graphene. Existing investigations of graphene nanocomposites obtained by FSP have studied the process, the microstructural and morphological characteristics, and some mechanical properties, but none has studied the tribological behavior of these materials.

In this study, the GNSs were dispersed by FSP in an aluminum alloy (AA1050). Metallographic examinations and wear tests, together with spectroscopic studies, were conducted on the surface of the GNSs/AA1050 composite, thereby contributing to the development of GNS-based nanocomposites via FSP.

2. Materials and Methods

To obtain the nanocomposite material, a sheet of aluminum AA1050 H24 and GNSs were used. The chemical composition (wt %) of the AA1050 H24 alloy was as follows: Al = 99.5, Si = 0.25, Fe = 0.40, Cu = 0.05, Mn = 0.05, Mg = 0.05, Zn = 0.07, Ti = 0.05, 0.03 corresponding to other elements. The GNSs used were supplied by the company *Avanzare Innovacion Tecnologica S.L.* The graphene supplied was obtained by the liquid phase exfoliation method. Morphologically, the flakes present average

dimensions of 250 nm in the XY plane, and an aspect ratio of 90:1. To complete the characterization, Scanning Electron Microscopy (SEM) and the Raman spectroscopy have been used.

The aluminum/GNS nanocomposites were obtained by means of the solid-state FSP process. The functioning principle of the process was described in [19,20]. For the trials, aluminum plates were used with dimensions of 200 mm long, 100 mm wide, and 3 mm thick. To place the GNS in the AA1050 plate, three grooves were made that were 2 mm wide and 0.5 mm deep, with a space of 3.5 mm between the grooves (Figure 1).

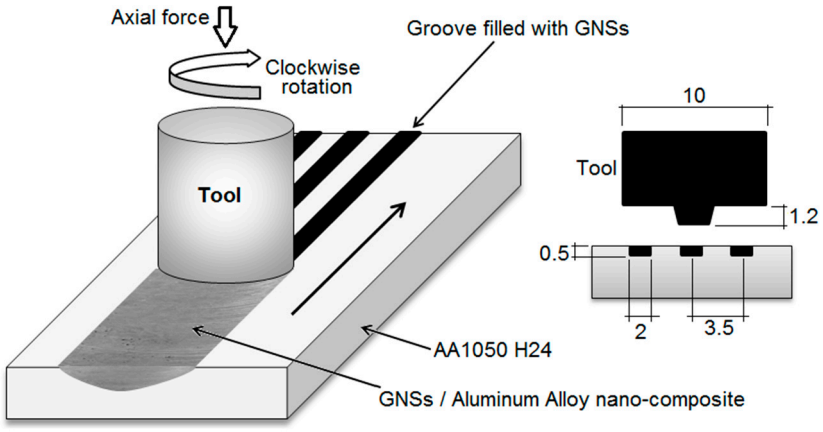

Figure 1. Schematics of the FSP process to manufacture GNS/AA1050 nanocomposites.

The tool used in the FSP process was a cylindrical probe with grooves that were 3 mm in diameter and 1.2 mm long [21]. The tool shoulder had a 10 mm diameter with a concave profile. The tool was made of AISI D2 steel. During the trials, two levels of tool rotation speed were used (1120 rpm and 1800 rpm), and the advancing speed of the tool was of 40, 63, and 100 mm/min.

To obtain microstructural optical images, the samples were cut in longitudinal and transverse sections, inserted in Bakelite, sanded with 220, 320, 400, 600, 1200, and 1500 grit sandpaper, and polished to a mirror finish with 6 µm and then 1 µm diamond paste. The polished samples were then etched using HF for 10 s. Following this chemical attack, an electrolytic attack took place. The electrolyte selected for the attack was Barker (HBF_4 diluted in 50% water), with 40 V voltage and a current of 0.5 A. The aluminum samples were used as a cathode. Images of the treated surfaces were obtained with an optical microscope Leica DMILM (Camera Leica EC3) with polarized light.

Raman spectra were made after and before wear test in different zones of the surface samples in the friction stir processed region, to confirm that the composite GNSs/AA1050 was obtained. Raman spectroscopy measurements were made using a Thermo Fisher DXR Raman Microscope with OMNICxi Raman Imaging software 1.0, as well as an incident laser light with wavelength and power of 532 nm and 3 mW, respectively. The Raman spectrum of clean Al alloy only presented a fluorescence background, which was used for background subtraction of the composite spectra.

The surfaces of the composite GNS/AA1050 were examined using a ZEISS EVO MA 15 SEM to reveal the presence of GNSs in the aluminum matrix. Microanalyses by means of Energy Dispersive X-ray Spectroscopy (EDS) and chemical mapping of the surface micro-regions were conducted in order to corroborate the presence of GNSs in the composite material GNS/AA1050.

The wear tests were performed in a Block-on-Ring Friction Pair tribometer, according to ASTM G77-05 Standard [22]. The ring was made with AISI 1020 steel with a polished surface finish. The block was made of the aluminum AA1050 with the nanocomposite surface GNS/AA1050 obtained by FSP. All trials were repeated three times to ensure reproducibility of the results. No kind of lubrication was used during the wear tests. The controlled parameters were: duration of wear tests of 30 min, constant load of 100 N, and an advancing speed of 2.5 mm/s. Previous to the wear tests, all wear contact surfaces of the nanocomposite material were mechanically polished to an average roughness

(Ra) of 0.1 ± 0.03 µm. Samples were cleaned with acetone and weighed before and after wear tests, to determine the mass loss, using an electronic balance with an accuracy of ±0.1 mg.

To measure the variables during the tests, signals were captured by a National Instruments USB 6210 Data Acquisition System. Special Labview® software was developed for that. The friction coefficient was monitored by measuring the electric power consumed in the Block-on-Ring system. Current measurements were conducted using a current transformer TA 210 and an I-U Amperflex converter. During the tests, the contact temperature of the test tube was monitored. All signals were acquired at a sampling frequency of 100 Hz.

3. Results and Discussion

3.1. GNS/AA1050 Composite Characterization

Figure 2a,b show an SEM image and the Raman spectrum of the GNSs, respectively. The SEM image shows that the GNSs have sizes ranging from some hundreds of nanometers (nm) up to some micrometers (µm). The Raman spectrum in Figure 2b has the typical shape of graphitic materials. The more intense features are the G peak at 1573 cm^{-1} and the 2D peak at about 2700 cm^{-1}. The G peak is due to the degenerate zone center E_{2g} mode, directly related to the C-C stretching modes in the two-dimensional graphene structure [23]. The 2D peak is the second order of the zone-boundary phonons, and its line-shape gives information on the number of graphene layers [24]. The inset in Figure 2b shows a fit of the 2D peak obtained by three Lorentzian functions. This finding indicates that GNSs have, predominantly, a thickness of 4 graphene layers [24]. Zone-boundary phonons do not satisfy the Raman fundamental selection rule, and are activated by defects, giving rise to the D peak located at 1345 cm^{-1}, which of course is absent in perfect graphene [23,25,26]. The I(D)/I(G) intensity ratio gives a qualitative measure of the density of defects, although this is to be taken with caution when the average lateral size of the graphene crystallites becomes very small [27]. It has to be noted that the peak intensity is intended as the height of the peaks. Another weak disorder-induced peak, called D′, is present on the high frequency side of the G peak, at about 1615 cm^{-1}. The D′ peak originates from an intravalley process in which the momentum conservation is satisfied by the presence of edges of the graphene crystallites [24]. It has been shown that the I(D)/I(D′) intensity ratio is related to the type of defects in large graphene crystallites [28]. The ratio has a maximum value of about 13 for sp^3 defects, decreases to a value of 7 for vacancy defects, and reaches a value of 3.5 for boundary defects. The fit of the spectrum in Figure 2b in the range of the D, G, and D′ peaks by Lorentzian curves allowed us to calculate a value of 3.2 for the I(D)/ID′) ratio, which means that the defects in GNSs are predominantly of boundary type. This finding, together with the SEM observation and with the conclusions made by fitting the 2D peak, gives us a quite complete description of the GNSs: they are flakes with lateral size of the order of hundreds of nanometers, with average thickness of four well-ordered graphene layers, showing only border-type defects. We also calculated a value of 0.17 for the I(D)/I(G) intensity ratio, which is consistent with the above conclusions [27]. The full width at half maximum (FWHM) of the D and G peaks is 36 cm^{-1} and 21 cm^{-1}, respectively.

Figure 2 shows (c) the SEM image and (d) the Raman spectrum of the GNS/AA1050 surface. The detail of the SEM image in Figure 2c shows that the original GNSs shown in Figure 2a were broken, associated with the high interaction of the tool with the material and the great plastic deformation resulting from the FSP process. The GNSs turned into nanosheets with smaller width (indicated by the arrows), which were homogeneously dispersed in the deformation bands of the processed material; this means that the flow of the deformed material dragged the smaller GNS nanosheets.

The Raman spectrum in Figure 2d shows the typical bands of graphitic materials, although noticeable difference has to be noted with respect to the spectrum of the GMSs in Figure 2b. In fact, a strong increase of the intensity of the D peak can be noticed, with a value of 1.5 for the I(D)/I(G) ratio, and an increase of the D′ intensity. Moreover, the FWHM of the D and G peaks is 74 cm^{-1} and 42 cm^{-1}, respectively, twice the values found in the GNSs case. The broadening of the D and G bands and the

increase of the I(D)/I(G) ratio indicate an increased degree of disorder in graphitic materials [26,29]. The intensity of the D′ peak increases, which means that the density of boundary-type defect increases, very likely due to a decrease of the average lateral size of the graphene crystallites. Moreover, the SEM image in Figure 2c suggests that some graphene flakes suffered a folding in the FSP process, resulting in the formation of tubular structures. Therefore, apart from the expected disorder induced by the friction stir process, our Raman spectra reveal a successful GNS/AA1050 mixture. Similar Raman results were reported in References [17,30].

It was observed that the tool rotation speed was the most influential factor in the variation of the morphology and dispersion of the GNS within the metallic matrix. A deeper study of the influence of the parameters of the FSP process on the morphology and dispersion of the GNS in the composite material must be conducted. As proved by Morisada et al. [16], the dispersion of nano-particles constitutes a factor that determines the thermo-physical, mechanical, and tribological behavior of composite materials.

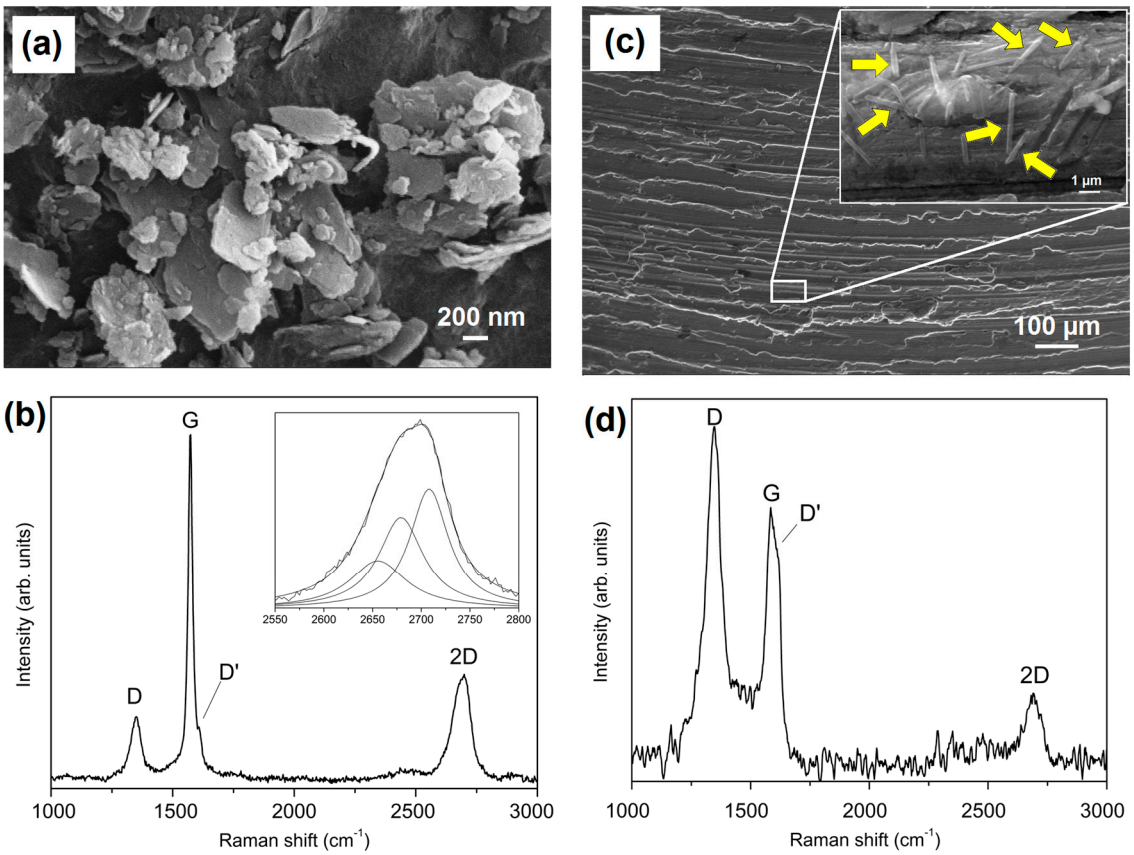

Figure 2. (**a**) SEM image and (**b**) Raman spectrum of the as-received GNSs. The inset in (**b**) shows the fit of the 2D peak by three Lorentzian functions; (**c**) SEM image and (**d**) Raman spectrum of the surface of the GNS/AA1050 composite obtained via FSP at 1800 rpm and 63 mm/min advancing speed. The inset in (**c**) shows the detail of the dispersion of the GNSs on the surface.

Figure 3 shows the transverse section of a sample of the GNS/AA1050 processed with 1120 rpm and 63 mm/min; the flawless processed region can be verified. The nanocomposite GNS/AA1050 obtained via FSP was free of macro-defects for all the tool rotation and advancing speed conditions.

Figure 3 also shows microscopic images of a processed sample, highlighting the stirred area of the nugget zone with fine recrystallized grains of the AA1050 matrix and in the cross section the deformation bands of the thermo-mechanically affected zone (TMAZ) typical of the FSP process.

The composite GNS/AA1050 was obtained in both areas. Also was shown the heat affected zone (HAZ) between base metal AA1050-H24 and TMAZ.

The zone delimited by a rectangle in Figure 3a is shown in different colors and in more detail in Figure 3b. Such enlargement allows us better appreciate the deformation bands of nanocomposite GNS/AA1050 material. Increasing the tool rotation speed up to 1800 rpm provokes a growth of recrystallized grains of the stir zone (SZ) [31]. This is due to the increased heat input of the friction between shoulder and pin of the tool with the material being processed. Therefore, it can be asserted that the tool rotation speed is more influential in the average grain size of the SZ.

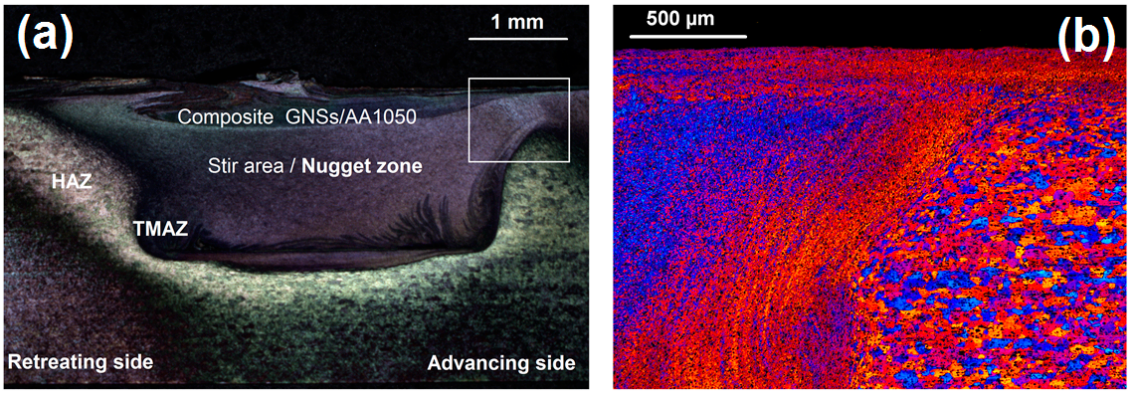

Figure 3. (**a**) Optical image of transverse section of the GNS/AA1050 nanocomposite obtained via FSP at 1120 rpm and 63 mm/min advancing speed; (**b**) enlargement of the zone delimited by the rectangle in (**a**).

The analyses undertaken in the SEM by EDS and chemical mapping helped to qualitatively confirm that the FSP process allowed us to obtain the nanocomposite material GNS/AA1050. Figure S1 (Supplementary materials) shows optical images of samples surface before and after FSP.

Figure 4 shows a SEM image of the surface of the composite material along with chemical mappings of the area delimited by a rectangle, and the EDS spectrum integrated on the whole area. Apart from the presence of O, Si, K, and Ca contaminants, the spatial distribution of the carbon signal confirms the presence of GNSs in the nanocomposite material.

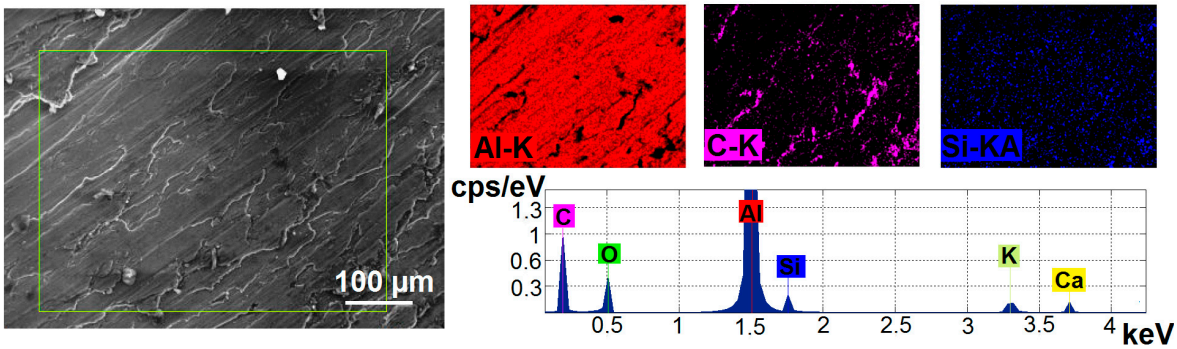

Figure 4. SEM image, EDS microanalysis and chemical mapping of the elements Al, C and Si of the surface of the composite material GNS/AA1050 obtained via FSP.

Table 1 shows the concentration of the elements in terms of the mass fraction wt % of that element in the sample. Although the EDS is not accurate for quantitative analyses of low atomic number elements (as C, O), the table only is provided as indicative information about the presence of C in the GNS/AA1050 composite.

Table 1. Results of EDS analysis of the representative sample.

El	AN	Series	unn. C [wt %]	norm. C [wt %]	Atom. C [wt %]	(1 Sigma) [wt %]
C	6	K-series	27.40	24.54	41.14	5.16
O	8	K-series	5.56	4.98	6.26	1.20
Na	11	K-series	0.22	0.20	0.17	0.05
Al	13	K-series	78.06	69.91	52.19	3.76
Si	14	K-series	0.21	0.19	0.14	0.04
K	19	K-series	0.11	0.10	0.05	0.04
Ca	20	K-series	0.10	0.09	0.05	0.04
		Total:	**111.65**	**100.00**	**100.00**	

3.2. Coefficient of Friction Evaluation

Figure 5 shows the behavior of the friction coefficient shown in the stable area, for all experimental conditions. It was observed that independently on the parameters of the FSP process (rotation and advancing speed), composite materials GNSs/AA1050 exhibit a lower friction coefficient with respect to the aluminum alloy AA1050.

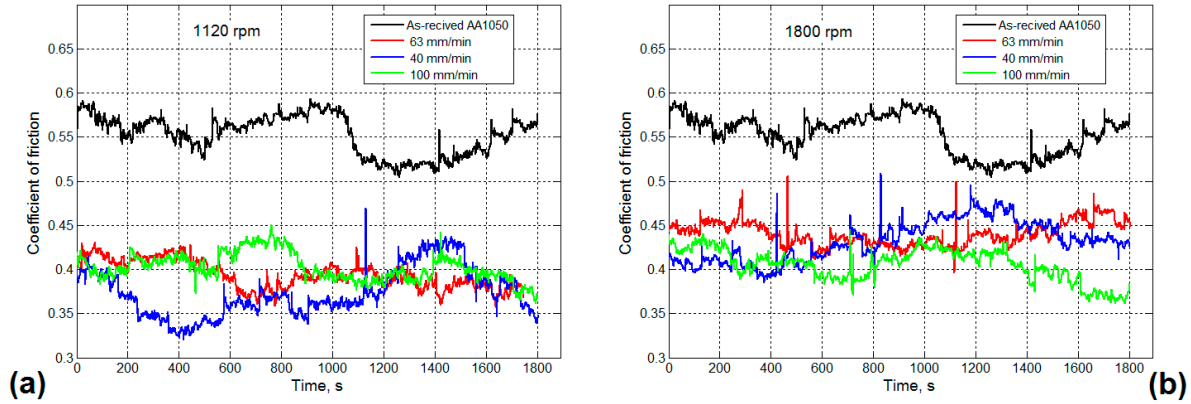

Figure 5. Friction coefficient of the composite material GNS/AA1050 obtained with three advancing speeds: (**a**) tool rotation speed 1120 rpm; (**b**) tool rotation speed 1800 rpm.

In Figure 5 it also can be noted that tool rotation speed influences the behavior of the friction coefficient of the composite materials obtained by FSP. The lower values of the friction coefficient were obtained in the materials processed with 1120 rpm, independent of the tool advancing speed in FSP. This is directly related to the effects of the matrix of the recrystallization process on the microstructure that occurs in the stirred zone, and with the dispersion of the GNSs in the matrix of the aluminum alloy.

The GNSs present in the nanocomposite decrease the contact surface with the steel disc, which leads to a decrease in the friction coefficient. Graphene has a hexagonal structure, with carbon atoms strongly connected in the basal planes by covalent bonds. However, in multilayer graphene adjacent planes are bonded by Van der Waals forces, which are weak and break easily when subjected to low shear loads. In other words, low shear forces lead to a displacement of the basal planes with respect to each other, decreasing the friction coefficient.

The results obtained confirm that the dispersion of nanoparticles is a factor that determines the thermo-physical, mechanical, and tribological behavior of composite materials, as reported by other authors [15,27].

The reason for reducing the friction coefficient is the presence of graphene sheets residues between the contact surfaces and the occurrence of wear in the form of delamination. This type of wear occurs essentially by separating laminated layers of the surface where the plastic deformation by shear causes

the nucleation and growth of cracks that occur below the surface; these cracks eventually join, resulting in layered detachment from the surface.

3.3. Wear Studies

The accumulation of dislocations below the surface, due to the high plastic deformation resulting from the FSP followed by the wear process, results in the formation of gaps in the region. These gaps can also be formed at the interface between graphene nanosheets and the matrix, due to the absence of chemical links between graphene and aluminum. The union of these gaps leads to the formation of cracks and the subsequent growth of debris during the wear process in the form of delaminated plates.

Figure 6a,b show SEM micrographs of worn surfaces of the AA 1050 alloy and the composite material GNSs/AA1050, respectively.

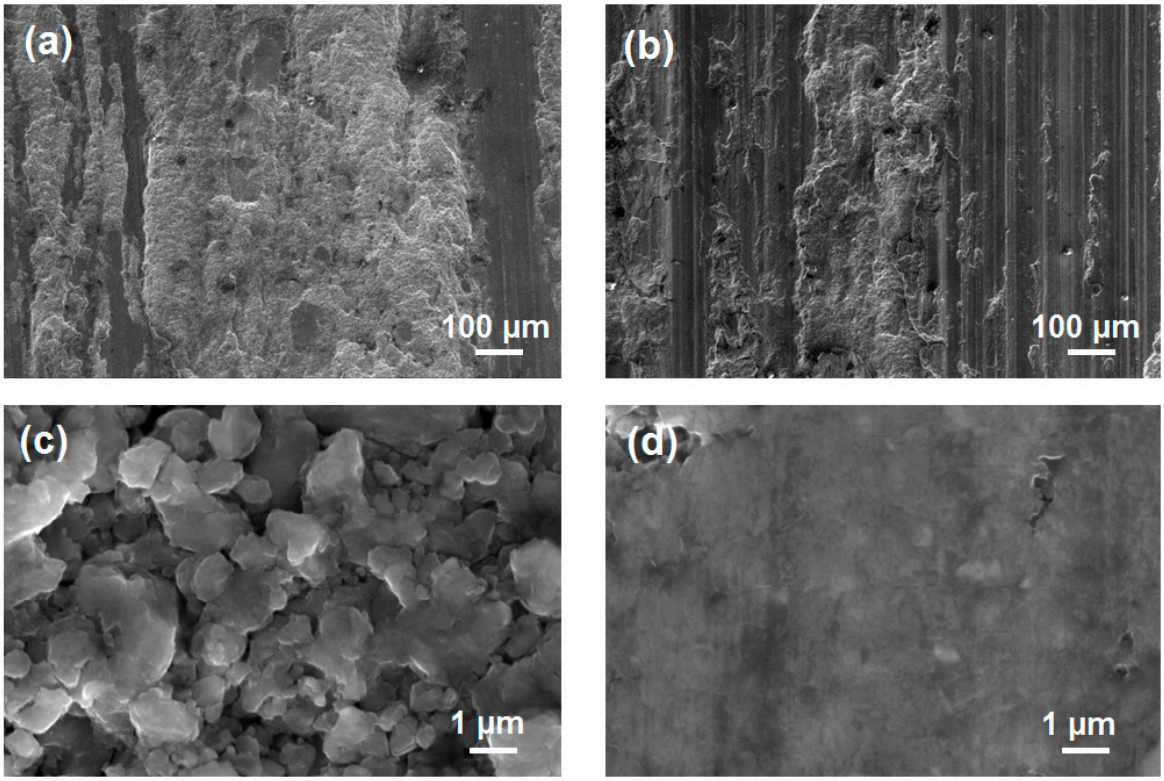

Figure 6. SEM images of the wear surfaces. (**a**) Wear surface aluminum alloy AA1050; (**b**) wear surface of the composite material GNS/AA1050; (**c**) valleys of the worn surface of the GNS/AA1050; (**d**) crests of the worn surface of the GNS/AA1050.

Great damage can be seen in Figure 6a and Figure S2 (Supplementary materials), due to the plastic deformation of the adhesive wear. Probably a plastic deformation occurs in the contact point during the wear process. The area adjacent to the wear zone is hardened due to the repetitive deformation, resulting in the formation of micro-cracks. These micro-cracks grow and lead to a detachment of the surface layer and, as a result, heavy adhesive wear occurs, with high friction coefficient and increased wear.

In the SEM image of the wear surface of the composite material GNSs/AA1050, shown in Figure 6b, it can be seen that areas of damage by severe plastic deformation are smaller and also have the typical grooves of this wear process. During the wear process, when the composite GNSs/AA1050 hits the counterpart steel AISI1020, the increase of the temperature at the interface favors the formation of friction micro-welding, causing an increase of the friction coefficient and the wear rate. Subsequently, and depending on the process dynamics, the GNS nanosheets detach and break and, in conjunction

with metal particles resulting from the wear process, form a film between the contact surfaces. Figure 6c,d show the valleys and the crests of the worn surface, respectively.

The formed film decreases direct contact friction between the two surfaces of the composite GNS/AA1050 and AISI 1020; therefore, the friction coefficient and the wear rate are reduced, and the wear stability is improved, as shown in Figure 5.

The wear process deforms plastically the matrix of the GNS/AA1050 composite, and thus probably tends to eject graphene nanoparticles to the displacement surface. Furthermore, the amount of graphene ejected towards the surface is probably related to the morphology of graphene, to the temperature at the displacement surface, and most importantly, to the link between the particles of graphene and the matrix. Since the FSP occurs at temperatures below the melting point of aluminum (below 650 °C), and due to the low solubility of carbon in solid aluminum, there is no chemical nor metallurgical link between the aluminum atoms and graphene, and the bond between them can only be achieved by mechanical joining [3]. Therefore, the separation of graphene particles to the displacement surface occurs easily, and no considerable force is required. However, due to the fact that multilayer graphene can be exfoliated much more easily with respect to the aluminum matrix layers, the link between graphene and the matrix has less effect on the amount of graphene expelled out to the surface instead of the plastic deformability of the matrix.

Figure 7a shows an image of the worn surface of the composite material GNSs/AA1050 obtained via FSP for the condition of 1800 rpm of tool rotation speed and 63 mm/min of advancing speed.

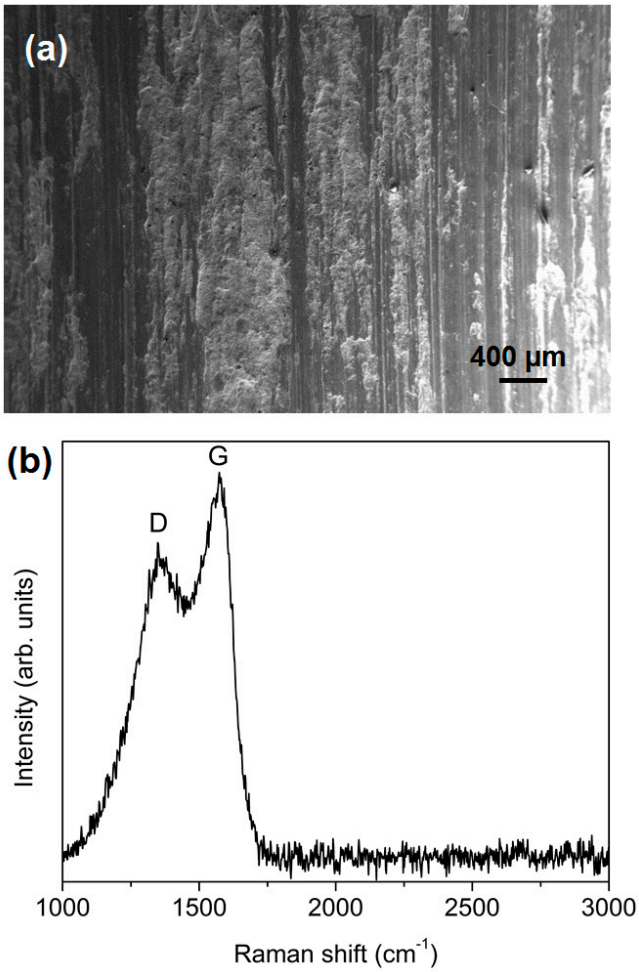

Figure 7. (**a**) SEM image and (**b**) Raman spectrum of the wear surface of the composite GNS/AA1050 obtained via FSP.

Figure 7b shows the Raman spectrum of the worn surface. The spectrum is quite different from the one shown in Figure 2d: the intensity of peak D is decreased with respect to peak G, and both show an increased broadening. Moreover, the 2D band is not present. A similar spectrum was measured on nano-graphite, obtained by ball milling of large flakes of graphene for 24 h, which introduces large amount of defects and breaks the crystallites into smaller particles [26]. The I(D)/I(G) ratio assumes a value of about 0.8, lower than the value obtained from the spectrum in Figure 2d. However, this is not an indication of a decrease of the density of defects in graphenic particles on the wear surface. For highly disordered graphenic materials, with average lateral sizes lower than 20 Å, the ratio has an inverse meaning, and the development of the D peak indicates ordering [27]. In fact, the D peak arises from aromatic rings, while the G peak is just related to the relative motion of carbon atoms in the sp^2 network. For increasing disorder, the distortion of the 2D structure leads to the opening of the rings, and the I(D) decreases with respect to I(G). Therefore, the difference between spectra in Figures 2d and 7b can be explained as due to a further fragmentation of the graphene particles due to the wear process.

The typical variation of the GNS/AA1050 composites weight loss with the changes in the FSP levels of tool rotation and advancing speeds is shown in Figure 8. As can be seen, the weight losses of the composites are less than that of unreinforced AA1050-H24 alloy for conditions with lower advancing speeds (40 and 60 mm/min) and 1120 rpm. The wear between the aluminum alloy AA1050 with processing by FSP and the steel counterpart AISI 1020 in the test Block-on-Ring occurred essentially by the adhesive mechanism, and therefore the friction coefficient and the degree of adhesive wear were high.

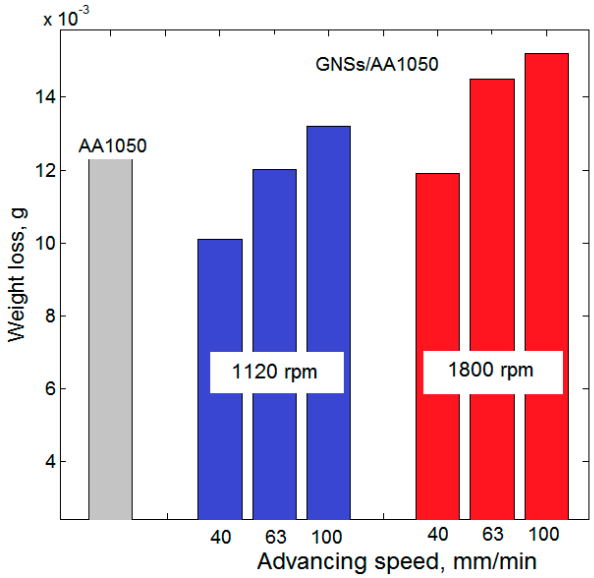

Figure 8. Weight loss of the AA1050-H24 alloy and the composite GNS/AA1050 as function of FSP parameters.

Figure 9 shows the SEM images of the wear debris, in which the nanoparticles indicated by the arrows are very likely GNS nanosheets, resulting from the film formed between the surfaces.

As mentioned above, graphene nanoparticles are expelled to the surface of the matrix during the displacement, forming a film on the interface between the contacting counterparts. With the increase in graphene content in the composite, this layer becomes thicker and denser, and it favors the reduction of the friction coefficient and wear rate. This layer is a mechanical mixture (Mixed Mechanical Layer/MML) and reduces the direct contact surface between the composite and the steel disk, and thus the friction coefficient and wear loss decrease. Aluminum, graphene, oxygen, moisture, and atmosphere are the components of the MML in the aluminum/graphene composite. As graphene

is a good lubricant, the presence of a small amount thereof makes the friction coefficient to be reduced (Figure 5). The graphene expelled to the surface forms separate groups (flakes—Figure 9) in the mixer layer. With the increase in the graphene content, the MML layer turns rich in graphene and the friction coefficient further decreases.

Obtaining, by means of FSP, a composite material of aluminum alloy AA1050, reinforced with GNSs, modified the wear mechanism of the material in the Block-on-Ring test. The wear occurred due to the surface delamination, decreasing the coefficient of friction and the wear rate of the material. This result confirms the performance of graphene as a lubricant, corroborated by other authors [6,7,10].

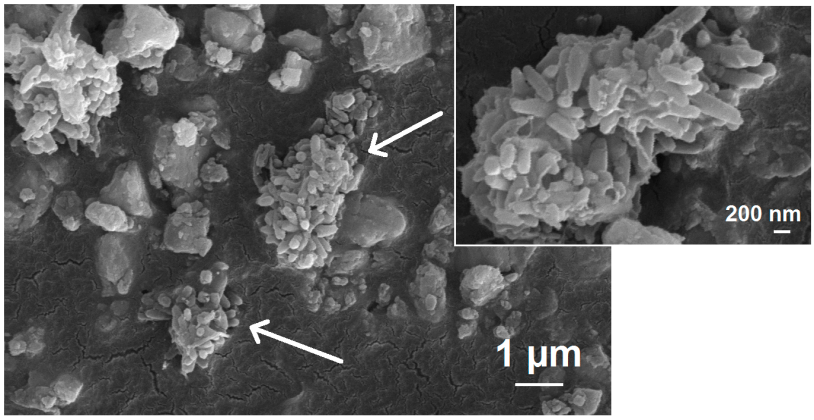

Figure 9. SEM image of the wear debris of the composite GNS/AA1050. A detail of agglomerated nanoparticles is shown on the right.

4. Conclusions

The present investigation allowed us to conclude that it is possible to obtain GNS/AA1050, with different values of the tool rotation and advancing speed. The results of Raman spectroscopy demonstrated that graphene nanosheets were successfully mixed with the aluminum matrix by FSP process. The friction coefficient of the composite was lower than that of the aluminum alloy AA1050, regardless of the FSP process parameters. This finding is very likely due to the detachment and to the fracture of the graphene particles in the wear process, forming a film that works as a lubricant and reduces the friction coefficient of the contacting materials. The friction coefficient was influenced by the tool rotation speed in FSP, being lower in the samples processed at 1120 rpm.

Supplementary Materials: The following are available online at http://www.mdpi.com/2075-4701/8/2/113/s1, Figure S1: Optical images of samples surface before and after FSP, Figure S2: SEM images of samples surface before and after FSP.

Acknowledgments: Authors thank the company *Avanzare Innovacion Tecnologica S.L.*, responsible for producing and supplying the GNSs used in this study.

Author Contributions: Julio Blanco Fernandez have designed and made the tools. Emilio Jiménez Macias has designed the process. Juan Carlos Saenz-Diez Muro has done the tests. Hipólito Domingo Carvajal Fals and Angel Sanchez Roca have analyzed properties of friction and metallurgy. Lorenzo Caputi, Domenico Miriello and Raffaella De Luca have analyzed microstructural images. Julio Blanco Fernandez, Hipólito Domingo Carvajal Fals and Lorenzo Caputi have reviewed and edited the manuscript.

Conflicts of Interest: The authors declare no conflict of interest.

References

1. Geim, A.K.; Novoselov, K.S. The rise of graphene. *Nat. Mater.* **2007**, *6*, 183–191. [CrossRef] [PubMed]
2. Park, S.; Ruoff, R. Chemical methods for the production of graphene. *Nat. Nanotechnol.* **2009**, *4*, 217–224. [CrossRef] [PubMed]

3. Wang, J.; Li, Z.; Fan, G.; Pan, H.; Chen, Z.; Zhang, D. Reinforcement with graphene nanosheets in aluminum matrix composites. *Scr. Mater.* **2012**, *66*, 594–597. [CrossRef]
4. Lee, C.; Wei, X.D.; Kysar, J.W.; Hone, J. Measurement of the elastic properties and intrinsic strength of monolayer graphene. *Science* **2008**, *321*, 385–388. [CrossRef] [PubMed]
5. Balandin, A.A.; Ghosh, S.; Bao, W.; Calizo, I.; Teweldebrhan, D.; Miao, F.; Lau, C.N. Superior thermal conductivity of single-layer graphene. *Nano Lett.* **2008**, *8*, 902–907. [CrossRef] [PubMed]
6. Zhao, W.; Zeng, Z.; Peng, S.; Dongwu, X.; Xue, Q.; Chen, J. Fabrication and investigation the microtribological behaviors of ionic liquid-graphene composite films. *Tribol. Trans.* **2013**, *56*, 480–487. [CrossRef]
7. Li-Yu, L.; Dae-Fun, K.; Whan-Kyun, K.; Seong-Chan, J. Friction and wear characteristics of multi-layer graphene films investigated by atomic force microscopy. *Surf. Coat. Technol.* **2011**, *205*, 4864–4869.
8. Shao, Z.; Sun, Y.; Liu, W.; Zhang, X.; Jiang, X. Effects of Multi-Phase Reinforcements on Microstructures, Mechanical and Tribological Properties of $Cu/Ti_3SiC_2/C/BN/GNPs$ Nanocomposites Sintered by Vacuum Hot-Pressing and Hot Isostatic Pressing. *Metals* **2016**, *6*, 324. [CrossRef]
9. Lim, D.K.; Shibayanagi, T.; Gerlich, A.B. Synthesis of multi-walled CNT reinforced aluminum alloy composite via friction stir processing. *Mater. Sci. Eng. A* **2009**, *507*, 194–199. [CrossRef]
10. Lee, C.H.; Wei, X.; Li, Q.; Carpick, R.; Kysar, J.W.; Hone, J. Elastic and frictional properties of grapheme. *Phys. Status Solidi B* **2009**, *246*, 2562–2567. [CrossRef]
11. Bertolucci, S.F.; Paras, J.; Rafiee, M.A.; Lee, S.; Kapoor, D.; Koratkar, N. Graphene-aluminum nanocomposites. *Mater. Sci. Eng. A* **2011**, *528*, 7933–7937. [CrossRef]
12. Tjong, S.C. Recent progress in the development and properties of novel metal matrix nanocomposites reinforced with carbon nanotubes and graphene nanosheets. *Mater. Sci. Eng. R* **2013**, *74*, 281–350. [CrossRef]
13. Mishra, R.S.; Ma, Z.Y.; Charit, I. Friction stir processing: A novel technique for fabrication of surface composite. *Mater. Sci. Eng. A* **2003**, *341*, 307–310. [CrossRef]
14. Liu, Q.; Ke, L.; Liu, F.; Xing, L. Microstructure and mechanical property of multi-walled carbon nanotubes reinforced aluminum matrix composites fabricated by friction stir processing. *Mater. Des.* **2013**, *45*, 343–348. [CrossRef]
15. Izadi, H.; Gerlich, A.P. Distribution and stability of carbon nanotubes during multi-pass friction stir processing of carbon nanotube/aluminum composites. *Carbon* **2012**, *50*, 4744–4749. [CrossRef]
16. Morisada, Y.; Fujii, H.; Nagaoka, T.; Fukusumi, M. MWCNTs/AZ31 surface composites fabricated by friction stir processing. *Mater. Sci. Eng. A* **2006**, *419*, 344–348. [CrossRef]
17. Li, Q.; Lee, C.; Carpick, R.W.; Hone, J. Substrate effect on thickness-dependent friction on graphene. *Phys. Status Solidi B* **2010**, *247*, 2909–2914. [CrossRef]
18. Deng, Z.; Klimov, N.N.; Solares, S.D.; Li, T.; Xu, H.; Cannara, R.J. Nanoscale interfacial friction and adhesion on supported versus suspended monolayer and multilayer graphene. *Langmuir* **2013**, *29*, 235–243. [CrossRef] [PubMed]
19. Jeon, C.H.; Jeong, Y.H.; Seo, J.J.; Tien, H.N.; Hong, S.T.; Yum, Y.J.; Hur, S.H.; Lee, K.J. Material properties of graphene/aluminum metal matrix composites fabricated by friction stir processing. *Int. J. Precis. Eng. Manuf.* **2014**, *15*, 1235–1239. [CrossRef]
20. Yong, X.G. Structural assessment of nanocomposites. *Micron* **2012**, *43*, 782–817.
21. Yan, S.J.; Dai, S.L.; Zhang, X.Y.; Yang, C.; Hong, Q.H.; Chen, J.Z.; Lin, Z.M. Investigating aluminum alloy reinforced by graphene nanoflakes. *Mater. Sci. Eng. A* **2014**, *612*, 440–444. [CrossRef]
22. ASTM G77-05. *Standard Test Method for Ranking Resistance of Materials to Sliding Wear Using Block-on-Ring Wear Test*; ASTM International: West Conshohocken, PA, USA, 2005.
23. Tuinstra, F.; Koenig, J. Raman spectrum of graphite. *J. Chem. Phys.* **1970**, *53*, 1126–1130. [CrossRef]
24. Malard, L.M.; Pimenta, M.A.; Dresselhaus, G.; Dresselhaus, M.S. Raman spectroscopy in graphene. *Phys. Rep.* **2009**, *473*, 51–87. [CrossRef]
25. Ferrari, A. Raman spectroscopy of graphene and graphite: Disorder, electron-phonon coupling, doping and nonadiabatic effects. *Solid State Commun.* **2007**, *143*, 47–57. [CrossRef]
26. Kaniyoor, A.; Ramaprabhu, S. A Raman spectroscopic investigation of graphite oxide derived graphene. *AIP Adv.* **2012**, *2*, 1–13. [CrossRef]
27. Ferrari, A.C.; Robertson, J. Interpretation of Raman spectra of disordered and amorphous carbon. *Phys. Rev. B* **2000**, *61*, 14095–14107. [CrossRef]

28. Eckmann, A.; Felten, A.; Mishchenko, A.; Britnell, L.; Krupke, R.; Novoselov, K.S.; Casiraghi, C. Probing the nature of defects in graphene by Raman spectroscopy. *Nano Lett.* **2012**, *12*, 3925–3930. [CrossRef] [PubMed]
29. Kudin, K.N.; Ozbas, B.; Schniepp, H.C.; Prud'homme, R.K.; Aksay, I.A.; Car, R. Raman spectra of graphite oxides and functionalized graphene sheets. *Nano Lett.* **2008**, *8*, 36–41. [CrossRef] [PubMed]
30. Orozco, M.S.; Jimenez Macias, E.; Sanchez Roca, A.; Carvajal Fals, H.D.; Blanco Fernandez, J. Optimization of friction-stir welding process using vibro-acoustic signal analysis. *Sci. Technol. Weld. Join.* **2013**, *18*, 532–540. [CrossRef]
31. Surekha, K.; Murty, B.S.; Rao, K.P. Effect of processing parameters on the corrosion behavior of friction stir processed AA2219 aluminum alloy. *Solid State Sci.* **2009**, *11*, 907–917. [CrossRef]